

## Optimization Using Response Surface Methodology for Biodiesel Production by Double-Pipe Static Mixer Reactor

Wissarut Attahiran<sup>1</sup>, Kulchanat Prasertsit<sup>1</sup>, Songtham Photaworn<sup>1\*</sup>

<sup>1</sup> Department of Chemical Engineering, Faculty of Engineering, Prince of Songkhla University, Hat Yai, Songkhla 90110, Thailand

\* Corresponding author's e-mail: [songtham.p@psu.ac.th](mailto:songtham.p@psu.ac.th)

### ABSTRACT

This study investigates continuous biodiesel production from refined palm oil (RPO) using a 250-cm-length double-pipe static mixer (DPSM), mixing elements were employed first with the low-pressure drop static mixer (LPD-SM) and second with the Kenics Static Mixer (K-SM). Four key independent parameters in the transesterification reaction – methanol (MeOH) to RPO molar ratio, KOH concentration, static mixer length, and residence time – were optimized to achieve the desired methyl ester content (%E, wt.%), set at 96.5 wt.%. From response surface methodology (RSM), The optimal conditions of LPD-SM were MeOH to RPO molar ratio at 5:1, KOH concentration at 0.76 wt.% of RPO, 250 cm static mixer length, and 7.7 min residence time. Conversely, K-SM showed optimal conditions with MeOH to RPO molar ratio at 5.5:1, KOH concentration at 0.81 wt.% of RPO, 250 cm static mixer length, and 7.2 min residence time. Statistical analysis revealed KOH concentration as the most influential parameter, followed by residence time, static mixer length, and MeOH to RPO molar ratio, respectively. In summary, LPD-SM outperformed K-SM in reducing the amount of alcohol and catalyst consumption while maintaining %E at the set point, highlighting its potential as an efficient, sustainable approach for biodiesel production from RPO using a DPSM.

**Keywords:** biodiesel production, optimized, response surface methodology, static mixer, transesterification.

### INTRODUCTION

Concerns regarding fluctuating fuel prices, the depletion of fuel resources, and the utilization of non-environmentally friendly resources are significant factors that require attention to ensure sustainability in fuel energy usage [1, 2]. Additionally, the concentration of oil resources in specific regions presents challenges in meeting energy demands for countries with limited oil production, necessitating reliance on external sources, subject to the political stability of these regions [3]. Moreover, the rising cost of petroleum products exacerbates this issue [4]. Acknowledging the challenges associated with traditional fuels, the adoption of renewable alternative fuels, particularly environmentally friendly options like biofuels, becomes imperative [5].

Biofuel sources are characterized by their cleanliness, environmental friendliness,

and the resulting reduction in greenhouse gas (GHG) emissions [6, 7, 8]. In the industrial and transportation sectors, biofuels have been identified as an appealing solution to enhance energy security, reduce the reliance on fossil fuels in these sectors, and consequently, mitigate the environmental impacts associated with fossil fuels [9]. Among the various biofuels currently available, biodiesel is preferred due to its numerous desirable characteristics. It is biodegradable, sustainable, and possesses attractive specifications such as a high calorific value, low sulfur content, lubrication ability, and a high cetane number [10].

Biodiesel is derived from biological sources such as vegetable oils or animal fats [11]. Its production involves a chemical reaction known as transesterification reaction [12], wherein these feedstocks are reacted with a suitable alcohol (typically methanol or ethanol) in the presence of

a suitable catalyst [13]. Depending on this reaction, the catalyst used can be an acid, base, or enzyme [14]. This reaction transforms the Triglyceride (TG) into biodiesel, also known as fatty acid alkyl ester (FAAE), and glycerol as a by-product [15]. Methanol (MeOH) is the most utilized alcohol for producing biodiesel in terms of fatty acids methyl ester (FAME) due to its cost-effectiveness and high reactivity [16, 17].

The transesterification reaction between TG and alcohol occurs through a series of three successive reversible steps [18], as represented in Eq. (1) to Eq. (3), respectively. The transesterification reaction, encompassing all three steps, can be described by Eq. (4).

*Catalyst*



Transesterification reaction:

*Catalyst*



where: MG, DG, and TG are mono-, di-, and triglyceride, respectively.

In traditional biodiesel production, the widely adopted reactor for commercial use is the continuous stirred tank reactor (CSTR) [19, 20, 21]. However, this reactor comes with its own set of limitations, including prolonged residence times, high molar ratios of alcohol to oil, and high operational and maintenance costs [22, 23]. The limitations of traditional biodiesel production highlight a critical need for an enhanced design in continuous processes to improve the efficiency of biodiesel production.

The simplest chemical reactor is the tubular reactor, also known as an in-line mixing or static mixer (SM) [8]. In this reactor, reactants are introduced at one end, flow through a pipe at a constant volumetric flow rate, spend a specific amount of time inside the pipe, and mix as they pass through the mixing element inside the pipe toward the outlet. SM offers several advantages for fluid mixing applications, including addressing the challenge of non-dilution of alcohol with oil to overcome the limitations of traditional biodiesel production [24]. Additional advantages of SM include its compact design, allowing for space-saving installations, low maintenance

costs, and energy-savings in the reactor due to the absence of moving parts [8].

The suitable mixing element achieves the desired mixing quality with the least pressure drop, ensuring minimal energy consumption. Examples of mixing elements include the lightning static mixer (L-SM) or the Kenics static mixer (K-SM), both widely employed in traditional industrial-scale biodiesel production [20, 25, 26].

In the literature review on biodiesel production using SM, an optimization study for continuous methyl ester production through transesterification was conducted by Somnuk et al. [27]. A 10 m length K-SM with refined palm oil (RPO) was employed. Optimal conditions included a 10:1 molar ratio of MeOH to RPO, 1.26 wt.% catalyst concentration, and 4.8 m length K-SM, achieving 96.87 wt.% methyl ester content (%E). In the study by Pongraktham and Somnuk [28], on continuous biodiesel production, a 1-m-length L-SM with RPO was employed. Optimal conditions included a 5.6:1 molar ratio of MeOH to RPO, 1.34 wt.% catalyst concentration, achieving %E of 45.04 wt.%. Moreover, the results demonstrated that lower length-to-diameter (L/D) ratios of mixing elements (e.g., K-SM and L-SM) result in higher purities of biodiesel products.

Another high-performance type of mixing element is the low-pressure drop static mixer (LPD-SM), which has demonstrated superior results in terms of reduced pressure drop. Through simulation via computational fluid dynamics (CFD), LPD-SM showcased advantages in mixing, reduced energy consumption [29], resident time [30], and exhibiting a low-pressure drop when compared to various mixing elements. This characteristic makes LPD-SM suitable for processes and reactions with brief residence times, particularly advantageous for biodiesel production, given the rapid nature of transesterification reactions [30]. The literature review suggests that LPD-SM holds significant promise for enhancing biodiesel production. While numerous researchers have utilized CFD to simulate experimental outcomes, a limited number of studies have exclusively focused on practical experiments involving continuous processes with LPD-SM. This research decision to opt for LPD-SM is driven by this observation.

To investigate and compare the factors influencing the purity of biodiesel in comparison to LPD-SM, the traditional mixing element, K-SM, was chosen as the comparator. Previous studies have affirmed the suitability of

K-SM for biodiesel production [20, 24, 27], and K-SM is widely recognized as one of the most commonly used industrial-scale mixing elements [25].

In this article, thirty experiments were designed using central composite design (CCD), and Response Surface Methodology (RSM) was employed to analyze the experimental data. The primary objective was to develop and utilize a regression RSM model to predict the optimal conditions for biodiesel production with LPD-SM and K-SM. All experiments for continuous biodiesel production were performed using LPD-SM compared with K-SM, with an overall SM length of 250 cm, employing RPO and MeOH as reactants, and potassium hydroxide (KOH) as a catalyst. The four independent factors varied in this experiment included the molar ratio of MeOH to RPO in the range of 4:1 to 6:1, the KOH concentration from 0.4 to 1 wt.% of RPO, the SM length spanning 100 to 250 cm, and the residence time ranging from 2 to 10 min. The fuel properties of %E from the optimal conditions were subsequently tested following the European Standardization (EN14124).

## MATERIALS AND METHODS

### Materials

Refined palm oil (RPO) was sourced from the Specialized Research and Development Center for Alternative Energy from Palm Oil and Oil Crops, Prince of Songkla University. The RPO had a free fatty acids (FFAs) content of approximately 0.3 wt.%, determined using standardized methods outlined by the American Oil Chemists' Society (AOCS). The remaining physical properties of the RPO are detailed in Table 1, while Table 2 presents the FFAs profile, determined

through gas chromatography with flame ionization detection (GC/FID).

All chemicals used in the experiments, including the commercial-grade 99.85 wt.% methanol (MeOH) purchased from Top Solvent Company (Thailand), 95 wt.% potassium hydroxides (KOH) obtained from ST Chemical Business, sodium hydroxide (NaOH) ordered from Loba Chemie Pvt. Ltd. (India), and hydrochloric acid (HCl) obtained from J.T. Baker (USA), were utilized.

### Double-pipe static mixer

Figure 1 provides a detailed illustration of a double-pipe static mixer (DPSM) and its associated mixing elements, constructed using stainless steel 304 (SS304). In this experimental setup, two types of mixing elements were contained in the inner pipe (static mixer pipe; SM pipe). The first type was a low-pressure drop static mixer (LPD-SM), and the second was a Kenics static mixer (K-SM), both constructed from SS304 with a length-to-diameter ratio (L/D) of 1.0. The LPD-SM element comprised two semi-elliptical plates connected at their centers, forming a perpendicular arrangement [25]. The edges of each element were welded together to ensure a secure connection [31, 32]. For the construction of the K-SM, each element was twisted 180° and connected to the next mixing element at a 90° angle [25, 26]. Additional specifications and geometrical details of the mixing elements are provided in Table 3.

### Experimental procedure of DPSM

Figure 2 illustrates a schematic diagram of the experimental setup used for the continuous transesterification process employing a DPSM. In preparation for initiating the experiment, the RPO was preheated to a temperature of 60 °C using a 1,000 W submerged heater (HT) situated within the RPO storage tank (T1). Following preheating,

**Table 1.** Physical properties of RPO

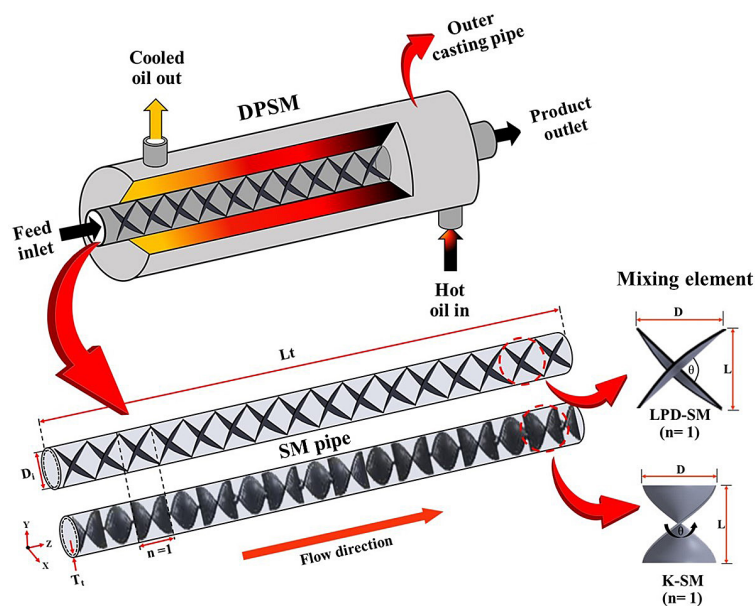
Property	Unit	RPO	Analysis method
Mean molecular weight	g/mol	850.41	Calculated <sup>a</sup>
Tri-glyceride (TG)	wt. %	98.46	TLC/FID <sup>b</sup>
Di-glyceride (DG)	wt. %	1.22	TLC/FID <sup>b</sup>
Mono-glyceride (MG)	wt. %	0.04	TLC/FID <sup>b</sup>
FFAs	wt. %	0.3	AOCS-Ca-5a-40

**Note:** <sup>a</sup> The mean molecular weight was calculated from the FFAs profile in RPO as shown in Table 2.

<sup>b</sup> The analysis was conducted using thin-layer chromatography with flame ionization detection (TLC/FID).

**Table 2.** The FFAs profile in RPO

Common name	Fatty acids	Content (wt.%)
Capric acid	C10:0	0.0073
Lauric acid	C12:0	0.1040
Myristic acid	C14:0	0.8225
Pentadecylic acid	C15:0	0.0399
Palmitic acid	C16:0	38.4299
Palmitoleic acid	C16:1	0.2181
Margaric acid	C17:0	0.0872
Steric acid	C18:0	3.8234
Oleic acid	C18:1	41.6657
Linoleic acid	C18:2	10.3757
Alpha linolenic acid	C18:3	0.1599
Arachidic acid	C20:0	0.3329
Paullinic acid	C20:1	0.1689
Behenic acid	C22:0	0.0590
Lignoceric acid	C24:0	0.0704
Others	-	3.6353
Total FFAs		
Saturated FFAs	-	43.78
Unsaturated FFAs	-	52.59
The mean MW of FFAs		270.81 g/mol

**Figure 1.** Double-pipe static mixer, geometries of the sm pipe fitted, and geometries of mixing elements ( $n = 1$ )

the RPO was consistently introduced into the SM pipe through a Grundfos Alldos positive displacement pump (P1, model DDA 30-4 AR-PVC). For each trial, a catalyst solution was supplied to the DPSM and introduced into the SM pipe through another Grundfos Alldos positive displacement pump (P2, model DDC 6-10 A-PP), drawing from the catalyst solution storage tank (T2).

The two-inlet flow passed through a 250-cm-length of DPSM to facilitate the transesterification reaction to the product storage tank (T4), and samples were collected at designated points (A, B, C, and D – corresponding to 100, 150, 200, and 250 cm) once the reactor had reached a steady state (approximately 8-time of residence time). To achieve

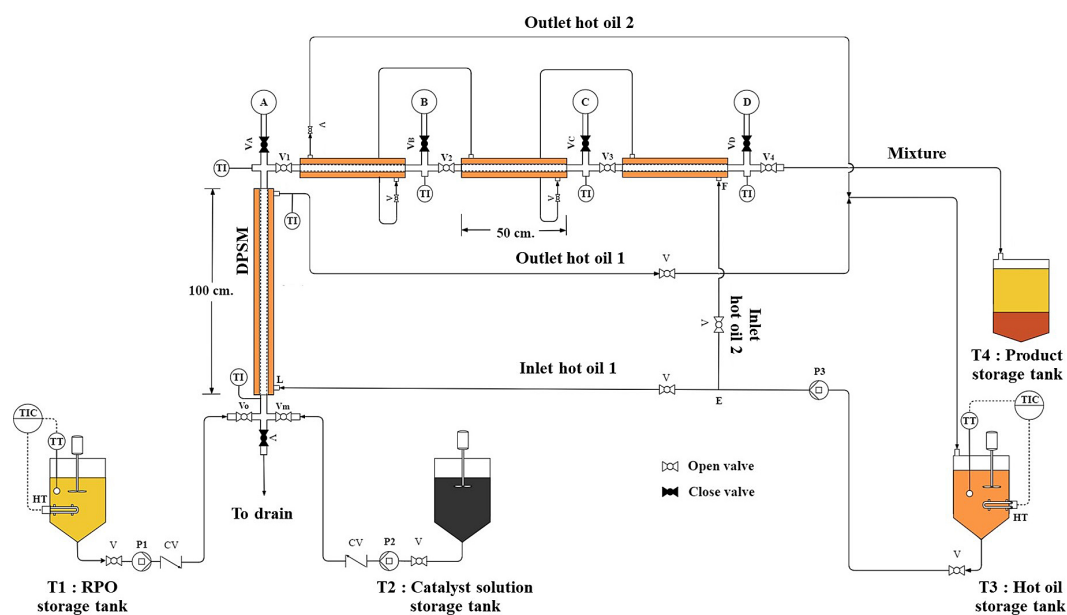


**Figure 2.** Schematic diagram of the experiment setup: T1 – RPO storage tank, T2 – catalyst solution storage tank, T3 – hot oil storage tank, T4 – product storage tank, HT – submerged heater, P1 – RPO continuous pump, P2 – catalyst solution continuous pump, P3 – hot oil circulating pump, DPSM – double-pipe static mixer, Vv – ball valve (VA, VB, VC, and VD – corresponding valve to take sample at 100, 150, 200, and 250 cm, V1, V2, V3, and V4 – corresponding shut valve to take sample at 100, 150, 200, and 250 cm), Vo – RPO valve, Vm – catalyst solution valve, CV – check valve, TI – temperature indicators, TT – temperature transmitters, TIC – temperature indicator controllers

**Table 3.** Specifications geometry of DPSM and mixing elements with an aspect ratio of  $L/D = 1.0$

Outer casting pipe		Symbol		Unit
Inner diameter		82.8		mm
SM pipe				
Overall length	$L_t$	100 <sup>a</sup>		cm
		150 <sup>b</sup>		cm
Inner diameter	$D_i$	22.5		mm
Thickness	$T_t$	2.1		mm
Mixing element ( $n = 1$ )		LPD-SM	K-SM	
Length	L	20	20	mm
Diameter	D	20	20	mm
Angle of twist	$\theta$	90°	180°	degree
Number	n	25 <sup>c</sup>	25 <sup>c</sup>	element
Thickness	-	2	2	mm

**Note:** <sup>a</sup> The position of the SM pipe in the vertical direction, <sup>b</sup> the position of the SM pipe in the longitudinal direction, and <sup>c</sup> the number of mixing elements per 50 cm of the SM pipe.

simultaneous control of the SM pipe temperature, dual hot oil was employed.

Samples were settled for 0.5 hours under each condition, resulting in two phases: the methyl ester (E) phase and the glycerol phase (G). Both phases underwent analysis for catalyst and soap content using the titration method. Subsequently, the resulting E phase was analyzed to determine its %E using thin-layer chromatography with flame ionization detection (TLC/FID).

### Experimental design

To optimize the biodiesel production using DPSM as a reactor, the %E was chosen as the response variable for the transesterification process. To evaluate %E and determine the optimal conditions, Response surface methodology (RSM) was employed. The axial parameter for rotatability ( $\alpha$ ) used in the experiment was expressed in Eq. (5).

$$\alpha = \sqrt[4]{2^k} \quad (5)$$

where:  $\alpha$  is the axial parameter for rotatability,  
 $k$  is the number of factors.

In this experiment, a five-level (-2, -1, 0, +1, and +2) and four-factor with central composite design (CCD) was utilized. The factors considered included the molar ratio of methanol to RPO (A), KOH concentration (K), static mixer length (L), and residence time (T), as detailed in Table 4. The combination of multiple regression analysis and analysis of variance (ANOVA) was performed to formulate a second-order polynomial equation predicting the response (%E). The general form of this equation is expressed as Eq. (6).

$$Y = \beta_0 + \sum_{i=1}^k \beta_i X_i + \sum_{j=1}^k \beta_{ii} X_i^2 + \sum_{i=1}^k \sum_{j=i+1}^k \beta_{ij} X_i X_j + \varepsilon \quad (6)$$

where:  $Y$  is predicted response (%E, wt.%),  $\beta_0$ ,  $\beta_i$ ,  $\beta_{ii}$  and  $\beta_{ij}$  are constant coefficients,  $X_i$  and  $X_j$  are the coded independent variables,  $k$  is the number of variables studied in this experiment,  $\varepsilon$  is the error.

## Analytical product

### Analysis of free fatty acids (FFAs)

The FFAs content of RPO was determined using the titrimetric method (AOCS Ca 5a-40). The percentage of FFAs in RPO was calculated using the relevant Eq. (7).

$$FFAs (\%) = \frac{(V \times C) \times 27.08}{w} \quad (7)$$

where:  $FFAs$  is free fatty acids content in RPO (%),  $V$  and  $C$  are the volume (mL) and molarity (M) of NaOH solution used in the titration method, respectively,  $w$  is the weight of RPO test portion (g), and 27.08 is the calculated number based on the mean molecular weight of FFAs.

### Analysis of remaining catalyst and soap content

The AOCS Cc 17-79 standard was used to determine the catalyst and soap contents in the E and G phases. The remaining catalyst and soap contents were calculated using Eq. (8) and Eq. (9), respectively.

$$ppm \text{ catalyst as KOH} = \frac{V_A \times C \times 56.1}{w} \times 1,000 \quad (8)$$

$$ppm \text{ soap as KOH soap} = \frac{V_B \times C \times 308.91}{w} \times 1,000 \quad (9)$$

where:  $V_A$  is the volume of HCl in the first titration (mL),  $V_B$  is the volume of HCl in the second titration (mL),  $C$  is the molarity of the HCl solution (M),  $w$  is the weight of the sample, and 56.1 and 308.91 (g/mol) represent the molecular weights of *KOH* and *KOH soap* with calculated from the data in Table 2, respectively.

### Analysis of %E

The %E was determined using a thin layer chromatography with flame ionization detection (TLC/FID). A TLC/FID (model: IATROSCAN MK-65; Mitsubishi Kagaku Iatron Inc., Tokyo, Japan) was used to analyze the %E in biodiesel. The equations used to calculate the %E [33] via TLC/FID were presented in Eq. (10).

$$\%E (\text{wt. \%}) = \frac{A_E}{\sum A_T} \times 100 \quad (10)$$

where: %E is methyl ester content (wt.%),  $A_E$  is the peak area of methyl ester (E), and  $\sum A_T$  is a summation of total peak areas.

## RESULTS AND DISCUSSION

### The experimental results of %E with DPSM

The objective of this experiment was to determine the optimal conditions for maximizing the %E with different types of mixing elements. These four factors – molar ratio of MeOH to RPO (A), KOH concentration (K), SM length (L), and residence time (T) – were represented as coded variables in Table 4. At the coded level (-2) for L, corresponding to 50 cm, a preliminary test revealed that the reaction did not occur at this length, resulting in a very low %E. Consequently, that run was eliminated, and a new run (Run no. 18) was substituted.

A total of 30 runs were conducted to investigate the responses, as outlined in Table 5. Notably, in almost all the runs, the %E of LPD-SM was greater than that of K-SM, as indicated by the positive values in the differential term (% $\Delta E$ ) calculated from Eq. (11).

$$\% \Delta E = \frac{[\%E_{LPD-SM} - \%E_{K-SM}]}{\%E_{LPD-SM}} \times 100 \quad (11)$$

where: % $\Delta E$  is percentage difference in %E between LPD-SM and K-SM,  $\%E_{LPD-SM}$  is the actual %E from the result of LPD-SM (wt.%),  $E_{K-SM}$  is the actual %E from the result of K-SM (wt.%).

**Table 4.** Central composite design algorithm for the transesterification process

Design summary (rotatable CCD, $\alpha = 2$ )							
Factors	4						
Total runs	30						
5-level factorial (full factorial) point types							
Non-center points	22						
Center points in cube	6						
Center points in axial	2						
Factors	Units	Symbol coded	Coded level				
			-2	-1	0	1	2
Molar ratio of MeOH to RPO	mol: mol	A	4	4.5	5	5.5	6
KOH concentration	wt.% of RPO	K	0.4	0.6	0.7	0.9	1
SM length	cm	L	50	100	150	200	250
Residence time	min	T	2	4	6	8	10

**Table 5.** The experimental design and results of the methyl ester content (%E) response for the transesterification process using DPSM

Run No.	Parameter				%E <sub>LPD-SM</sub>		%E <sub>K-SM</sub>		%ΔE Experimental
	A	K	L	T	(Y, wt.%)		(Y, wt.%)		
					Experimental	Predicted	Experimental	Predicted	
1	-2	0	0	0	70.88	70.46	72.07	72.49	-1.68
2	-1	-1	-1	-1	74.07	74.27	70.98	71.24	4.17
3	-1	-1	-1	+1	74.56	75.17	72.22	72.87	3.14
4	-1	-1	+1	-1	57.71	58.09	55.22	55.01	4.31
5	-1	-1	+1	+1	70.71	70.10	69.31	68.13	1.98
6	-1	+1	-1	-1	82.24	82.02	80.24	79.68	2.43
7	-1	+1	-1	+1	82.55	82.34	80.62	79.89	2.34
8	-1	+1	+1	-1	74.98	75.18	72.95	73.54	2.71
9	-1	+1	+1	+1	86.03	86.62	85.03	85.24	1.16
10	0	-2	0	0	35.18	35.14	29.35	29.27	16.57
11	0	0	0	-2	64.19	64.02	57.02	56.49	11.17
12	0	0	0	0	85.70	85.18	84.80	84.10	1.05
13	0	0	0	0	85.34	85.18	84.50	84.10	0.98
14	0	0	0	0	84.62	85.18	84.13	84.10	0.58
15	0	0	0	0	84.54	85.18	84.28	84.10	0.31
16	0	0	0	0	85.31	85.18	83.95	84.10	1.59
17	0	0	0	0	85.43	85.18	83.48	84.10	2.28
18	0	0	+1	0	84.13	83.93	81.94	82.50	2.60
19	0	0	+2	0	85.46	85.36	83.49	83.41	2.31
20	0	0	0	+2	80.43	80.45	74.21	74.80	7.73
21	0	+2	0	0	82.59	82.46	81.38	81.60	1.47
22	+1	-1	-1	-1	69.05	69.31	66.08	66.58	4.30
23	+1	-1	-1	+1	75.17	74.10	73.94	72.71	1.64
24	+1	-1	+1	-1	58.41	57.81	52.95	53.20	9.35
25	+1	-1	+1	+1	72.65	73.72	69.79	70.83	3.94
26	+1	+1	-1	-1	82.63	82.51	82.33	82.71	0.36
27	+1	+1	-1	+1	86.12	86.73	86.66	87.42	-0.63
28	+1	+1	+1	-1	80.05	80.37	79.68	79.42	0.46
29	+1	+1	+1	+1	96.64	95.71	96.46	95.62	0.19
30	+2	0	0	0	72.50	72.77	76.00	75.64	-4.83

**Note:** A is molar ratio of MeOH to RPO, K is KOH concentration, L is SM length, and T is residence time.

The  $\%E_{LPD-SM}$  ranged from 35.18 to 96.64 wt.%, while  $E_{K-SM}$  ranged from 29.35 to 96.46 wt.%. Run no. 29 exhibited the highest  $\%E$ , reaching 96.64 wt.% with LPD-SM and 96.46 wt.% with K-SM, respectively. This specific run utilized a molar ratio of MeOH to RPO of 5.5:1 mol: mol, KOH concentration of 0.9 wt.% of RPO, SM length of 200 cm, and a residence time of 8 min. In contrast, run no. 10 demonstrated the lowest  $\%E$ , measuring 35.18 wt.% with LPD-SM and 29.35 wt.% with K-SM. This run employed a molar ratio of MeOH to RPO of 5:1 mol: mol, KOH concentration of 0.4 wt.% of RPO, SM length of 150 cm, and a residence time of 6 min. These findings underscore the impact of the four factors and types of mixing elements on  $\%E$  in the transesterification process.

### Statistical analysis and predicted model

ANOVA was employed to analyze the data through multiple regression analysis to fit a second-order polynomial equation for biodiesel production with DPSM. The results of ANOVA, summarized in Table 6, indicate that the model was significant at a 95% confidence Interval (95%CI). Several parameters were considered to select the best-fitting model for both types of mixing elements, including the probability of error value (P-value), F-value, Lack-of-Fit (LOF), the coefficient of determination ( $R^2$ ), the adjusted coefficient of determination ( $R^2_{adj}$ ), and the predicted coefficient of determination ( $R^2_{pred}$ ) [34, 35].

The high  $F$ -values for the models of LPD-SM and K-SM in the ANOVA table (Table 6) were 624.92 and 533.70, respectively. These  $F$ -values are significantly higher than the critical  $F$ -value of 2.4243 at a significance level ( $\alpha$ ) of 0.05 (higher than  $F(\alpha, DF$  of model,  $DF$  of residual);  $F(0.05, 14, 15)$ ), which indicates that these models are accepted based on the  $F$ -value criterion [35].

Furthermore, the  $P$ -values of the models for both types of mixing elements were less than 0.0001. To accept the significance of these models, the  $P$ -value must be less than 0.05 at a 95%CI [35]. The observed  $P$ -values indicate a high level of significance for both models. The  $P$ -values of  $LOF$  for the LPD-SM and K-SM models were 0.1457 and 0.0613 higher than 0.05, respectively, which implied that the  $LOF$  was not significant relative to the pure error. A non-significant  $LOF$  was favorable, indicating that the predicted model adequately fit the data [34].

The quality of a regression model is assessed by the values of  $R^2$ ,  $R^2_{adj}$  and  $R^2_{pred}$ . The high  $R^2$  values of 99.83% (LPD-SM) and 99.80% (K-SM) indicate the acceptance of the model and the ability to fit the actual results well [36]. The  $R^2_{adj}$  and  $R^2_{pred}$  values for LPD-SM (99.67% and 99.10%) and K-SM (99.61% and 98.90%), respectively, are in reasonable agreement with each other. The high value of  $R^2_{adj}$  indicates that the RSM model regression yields a confidence value higher than 95% [36]. The very close values of  $R^2$  and  $R^2_{adj}$  with the difference being less than 20%, indicate a high level of reliability in the fit using the RSM model regression for the model [35]. RSM was employed to evaluate the fitted regression model for both mixing elements in predicting the  $\%E$  in coded terms during the continuous transesterification process using the DPSM.

The  $P$ -values must be lower than 0.05 to establish significance. However, upon examining the  $P$ -values of KOH concentration  $\times$  residence time (KT) from Table 6, the results revealed a value of 0.4047 for LPD-SM and 0.0944 for K-SM. Both values exceeded 0.05, signifying their statistical insignificance. Consequently, the term “KT” was eliminated from the model in Eq. (12) when compared to the other terms exhibiting a significant response.

The regression function was expressed as a second-order polynomial in multiple variables given by the following:

$$\%E = \beta_0 + \beta_1A + \beta_2K + \beta_3L + \beta_4T + \beta_5A^2 + \beta_6K^2 + \beta_7L^2 + \beta_8T^2 + \beta_9AK + \beta_{10}AL + \beta_{11}AT + \beta_{12}KL + \beta_{13}LT \quad (12)$$

where:  $\%E$  is the methyl ester content (wt.%),  $A$  is the molar ratio of MeOH to RPO,  $K$  is the KOH concentration,  $L$  is the SM length,  $T$  is the residence time and  $\beta$  is the coefficient value, as reported in Table 7.

The coefficients value in Table 7 offer valuable insights into the impact of different factors on  $\%E$ . When comparing the coefficient value of variables for biodiesel production with DPSM, it was evident that KOH concentration (K) had a highly significant effect compared to other parameters. The results aligned with the findings of other researchers who had found that the KOH concentration had a greater effect on the production purity of  $\%E$  [36]. Quadratic effect of K, residence time (T), and quadratic effect of molar ratio of MeOH to RPO (A) followed as the second, third, and fourth most influential factors,

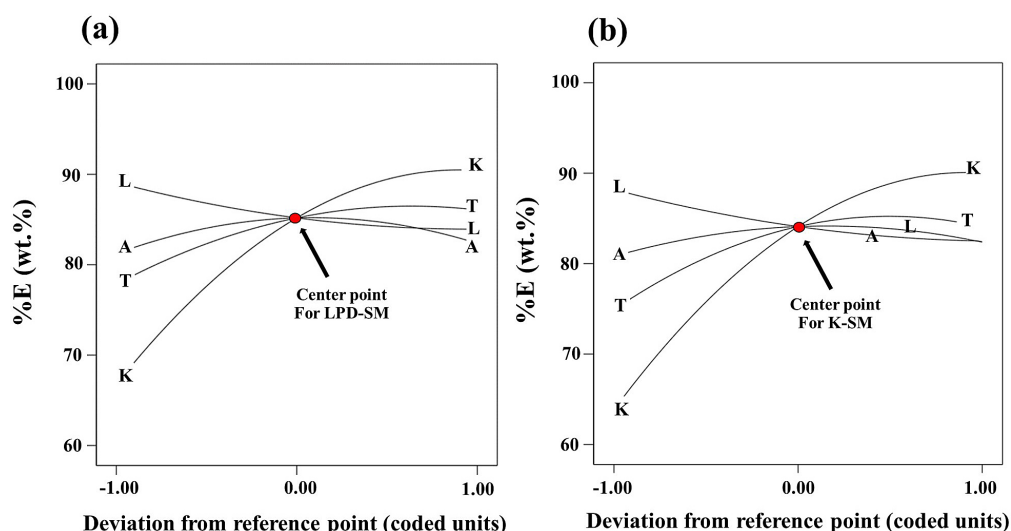


**Figure 3.** The perturbation plot displays the four influential factors on methyl ester content (%E) of biodiesel production by using DPSM: A – molar ratio of MeOH: RPO, K – KOH concentration, L – SM length, and T – residence time for (a) LPD-SM and (b) K-SM, respectively

**Table 6.** ANOVA for response surface model for the transesterification process using DPSM

Source	SS		DF		MS		F-Value		P-Value	
	LPD-SM	K-SM	LPD-SM	K-SM	LPD-SM	K-SM	LPD-SM	K-SM	LPD-SM	K-SM
Model	4040.54	4952.86	14	14	288.61	353.78	624.92	533.70	< 0.0001	< 0.0001
A	7.43	13.94	1	1	7.43	13.94	16.09	21.03	0.0011	0.0004
K	2854.55	3493.44	1	1	2854.55	3493.44	6180.91	5270.18	< 0.0001	< 0.0001
L	106.02	129.01	1	1	106.02	129.01	229.56	194.63	< 0.0001	< 0.0001
T	377.56	469.56	1	1	377.56	469.56	817.53	708.37	< 0.0001	< 0.0001
A <sup>2</sup>	315.75	172.75	1	1	315.75	172.75	683.69	260.61	< 0.0001	< 0.0001
K <sup>2</sup>	1285.07	1516.57	1	1	1285.07	1516.57	2782.54	2287.89	< 0.0001	< 0.0001
L <sup>2</sup>	28.00	24.59	1	1	28.00	24.59	60.62	37.10	< 0.0001	< 0.0001
T <sup>2</sup>	287.54	584.37	1	1	287.54	584.37	622.61	881.58	< 0.0001	< 0.0001
AK	30.99	61.26	1	1	30.99	61.26	67.1	92.42	< 0.0001	< 0.0001
AL	22.02	8.15	1	1	22.02	8.15	47.68	12.30	< 0.0001	0.0032
AT	15.19	20.30	1	1	15.19	20.30	32.89	30.62	< 0.0001	< 0.0001
KL	88.28	102.79	1	1	88.28	102.79	191.15	155.07	< 0.0001	< 0.0001
KT	0.3395	2.11	1	1	0.3395	2.11	0.7351	3.19	0.4047	0.0944
LT	123.6	132.14	1	1	123.6	132.14	267.63	199.34	< 0.0001	< 0.0001
Residual	6.93	9.94	15	15	0.4618	0.6629				
LOF	5.83	8.90	10	10	0.5832	0.8901	2.66	4.27	0.1457	0.0613
Pure error	1.10	1.04	5	5	0.2191	0.2083				
Total	4047.47	4962.80	29	29						
Model summary		LPD-SM	K-SM							
R <sup>2</sup>		99.83%	99.80%							
R <sup>2</sup> <sub>adj</sub>		99.67%	99.61%							
R <sup>2</sup> <sub>pred</sub>		99.10%	98.90%							

**Note:** DF is the degree of freedom, SS is the sum of square, MS is the mean of square, and LOF is the lack of fit.

respectively. The effectiveness rank can be shown with the coded parameters as  $\underline{K} > \underline{K}^2 > \underline{T} > \underline{A}^2 > \underline{T}^2 > \underline{LT} > \underline{L} > \underline{KL} > \underline{AK} > \underline{AL} > \underline{L}^2 > \underline{AT} > \underline{A}$ .

Figure 3 presents the results of the statistical analysis in the form of perturbation plots at the center point. These plots illustrate the comparative

effects of all independent variables across the studied range on the %E of biodiesel production using DPSM. A sharp curvature in the plot indicates high sensitivity of the response to that factor, whereas flat or semi-flat curvatures suggest insensitivity or less sensitivity [37]. Analyzing the perturbation plots in Figure 3(a) for LPD-SM and Figure 3(b) for K-SM, it can be inferred that the KOH concentration exhibits the highest sharp curvature, indicating the highest sensitivity to %E. The sensitivity of %E can be ranked in the following decreasing order:  $K \gg T > L > A$ .

Run no. 10 can be characterized by a low KOH concentration of 0.4 wt.% of RPO, compared to the center point experiment, which maintained a KOH concentration of 0.7 wt.% of RPO while holding other parameters constant. The %E increased from 35.18 to 85.13 wt.% for LPD-SM (approximately 2.4 times) and from 29.35 to 84.19 wt.% for K-SM (approximately 2.9 times) as the KOH concentration increased. These results indicate that KOH concentration exerted the strongest effect on biodiesel production using DPSM, as supported by both the actual experiments and the statistical analysis. Run no. 11, which featured a low residence time of 2 min, compared to the center point experiment, where the residence time was increased to 6 min while maintaining other parameters constant. The %E increased from 64.19 to 85.13 wt.% for LPD-SM (approximately 1.33 times) and from 57.02 to 84.19 wt.% for K-SM (approximately 1.47 times) as the residence time increased. Regarding the third-ranked factor, which pertains to the SM length, the results from Figure 3 suggest that increasing the length beyond optimal conditions does not significantly affect the increase in %E during the biodiesel production process with SM. This finding is consistent with the results of the study by Somnuk et al. [27], which indicated that increasing the SM length beyond optimal conditions while keeping other parameters constant did not significantly impact the increase in %E. Specifically, the results showed that %E only increased from 92.49 to 94.12 as the SM length increased from 2 to 8 m, respectively. The fourth-ranked factor pertains to the molar ratio of MeOH: RPO, as shown in Table 5, Run no. 1, where the molar ratio was 4:1, compared to the center point experiment, where it was increased to 5:1. The %E increased from 70.88 to 85.13 wt.% for LPD-SM (approximately 1.20 times) and from 72.07 to 76.00 wt.% for K-SM (approximately 1.05 times) as the molar ratio of MeOH: RPO increased.

In Table 7, it was observed that the quadratic forms of the parameters, particularly associated with the SM length (L) parameter, had the highest variance inflation factor (VIF) of 1.30. However, VIFs for other parameters were close to 1.00. The VIF serves as an indicator of the impact of multicollinearity (correlation between predictors) on the regression fit, influencing the variance of the regression coefficients [34]. Elevated multicollinearity can obscure the distinct effects of correlated predictors; a VIF greater than 5 typically signifies poorly estimated regression coefficients. In this analysis, the VIF values were considerably lower than 5 ( $VIF < 5$ ), indicating that acceptable estimation was achieved for the experimental data under consideration [34].

### Response surface plots and verification

In the transesterification with DPSM, three-dimensional (3D) response surface plots were utilized to demonstrate changes in %E by two varying parameters within their experimental range, while other parameters were maintained constant at their center point was depicted in Figure 4. In the selection of factors to be explained here, only those influencing the composition of the inlet substances and affecting the volumetric flow rate – specifically, the molar ratio of MeOH to RPO (A), the KOH concentration (K), and residence time (T) – are considered.

#### *The interaction effect between the molar ratio of MeOH to RPO and the KOH concentration*

The experiment provided insights into how changes in the molar ratio of MeOH to RPO (A) and the KOH concentration (K) affected the %E for LPD-SM and K-SM. At the center point ( $L = 150$  cm and  $T = 6$  min), an increase in the molar ratio of MeOH to RPO resulted in a rise in %E. Within the specified ranges (4:1 to 5:1 for LPD-SM and 4:1 to 5.3:1 for K-SM), as depicted in Figure 4(a) and Figure 4(b) for LPD-SM and K-SM, respectively. However, exceeding these ratios (beyond 5:1 for LPD-SM and 5.3:1 for K-SM) led to a lower %E due to a dilution effect that resulted in an incomplete reaction. This aligns with prior reports indicating that an excess of alcohol in the transesterification reaction (nearly 6:1 when using KOH as a catalyst) tends to decrease %E [38].

The product, resulting from the dilution effect, exhibited a three-layer structure: the top

**Table 7.** Coefficient value for the transesterification process using DPSM

Coefficients		Coefficients value		95% CI (low, high)		VIF	
terms		LPD-SM	K-SM	LPD-SM	K-SM	LPD-SM	K-SM
$\beta_0$		85.18	84.10	(83.43, 84.78)	(84.62, 85.74)	-	-
$\beta_1$	A	0.5759	0.7888	(0.4222, 1.16)	(0.2698, 0.8819)	1.07	1.07
$\beta_2$	K	11.83	13.09	(12.70, 13.47)	(11.51, 12.15)	1.22	1.22
$\beta_3$	L	-2.58	-2.85	(-3.28, -2.41)	(-2.94, -2.22)	1.30	1.30
$\beta_4$	T	4.11	4.58	(4.21, 4.95)	(3.80, 4.41)	1.07	1.07
$\beta_5$	A <sup>2</sup>	-3.39	-2.51	(-2.84, -2.18)	(-3.67, -3.11)	1.05	1.05
$\beta_6$	K <sup>2</sup>	-6.59	-7.16	(-7.48, -6.84)	(-6.86, -6.33)	1.24	1.24
$\beta_7$	L <sup>2</sup>	1.34	1.25	(0.8142, 1.69)	(0.9705, 1.70)	1.17	1.17
$\beta_8$	T <sup>2</sup>	-3.24	-4.61	(-4.94, -4.28)	(-3.51, -2.96)	1.05	1.05
$\beta_9$	AK	1.37	1.92	(1.50, 2.35)	(1.01, 1.72)	1.07	1.07
$\beta_{10}$	AL	1.37	1.92	(1.50, 2.35)	(1.01, 1.72)	1.07	1.07
$\beta_{11}$	AT	0.9744	1.13	(0.6924, 1.56)	(0.6123, 1.34)	1.00	1.00
$\beta_{12}$	KL	2.34	2.52	(2.09, 2.95)	(1.98, 2.70)	1.10	1.10
$\beta_{13}$	LT	2.78	2.87	(2.44, 3.31)	(2.42, 3.14)	1.00	1.00

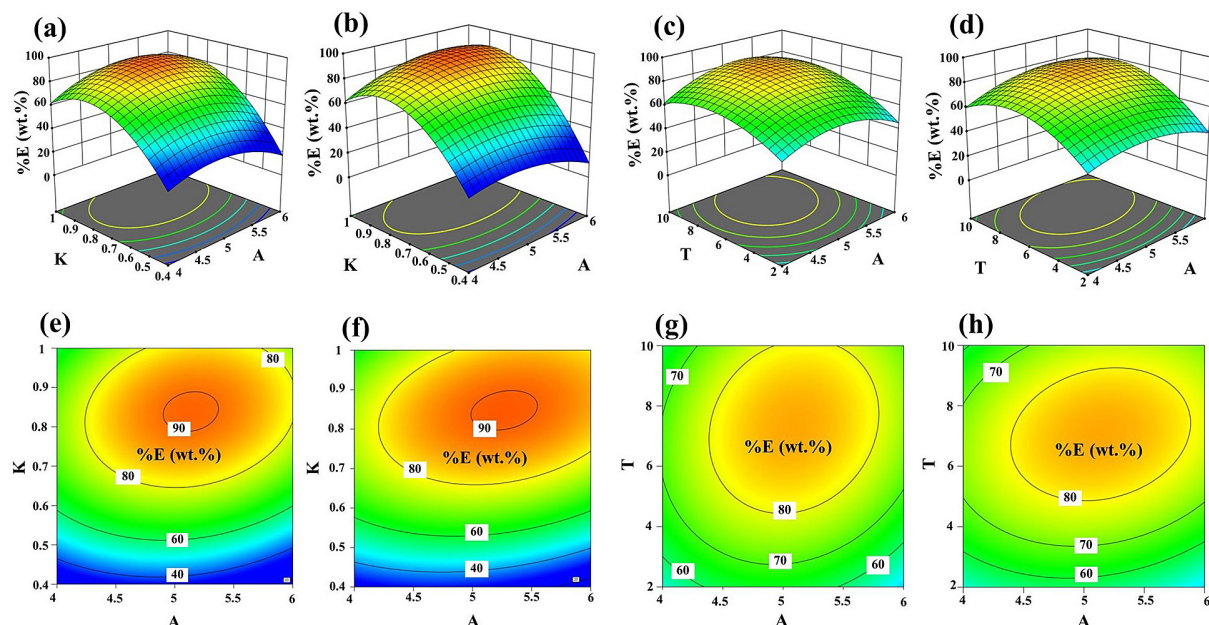


**Figure 4.** Response surface and contour plots depicting the relationship between methyl ester content (%E) and independent parameters in biodiesel production using DPSM at the center point: (a) and (b) response surface plots illustrating the %E to the effect of A × K for LPD-SM and K-SM, respectively; (c) and (d) response surface plots illustrating the %E to the effect of A × T for LPD-SM and K-SM, respectively; (e) and (f) contour plots illustrating the %E to the effect of A × K for LPD-SM and K-SM, respectively; (g) and (h) contour plots illustrating the %E to the effect of A × T for LPD-SM and K-SM, respectively

layer comprised an excess of the alcohol phase (Alc), the middle layer was the E phase, and the bottom layer was the G phase. In contrast, the typical product from the transesterification reaction displayed only the E and G phases [39] (Figure 5). It was evident from this work that the product exhibited a three-layer structure, leading to a lower %E.

Initially, an increase in KOH concentration boosted %E. However, beyond a threshold ( $0.4 \leq K \leq 0.9$  wt.%), it had a negative impact on both mixing elements. This trend was illustrated in the contour plot as depicted in Figure 4(e) and Figure 4(f) for LPD-SM and K-SM, respectively, where %E increased from run no. 10 (A = 5:1 mol MeOH: mol RPO, K = 0.4 wt.% of RPO, L

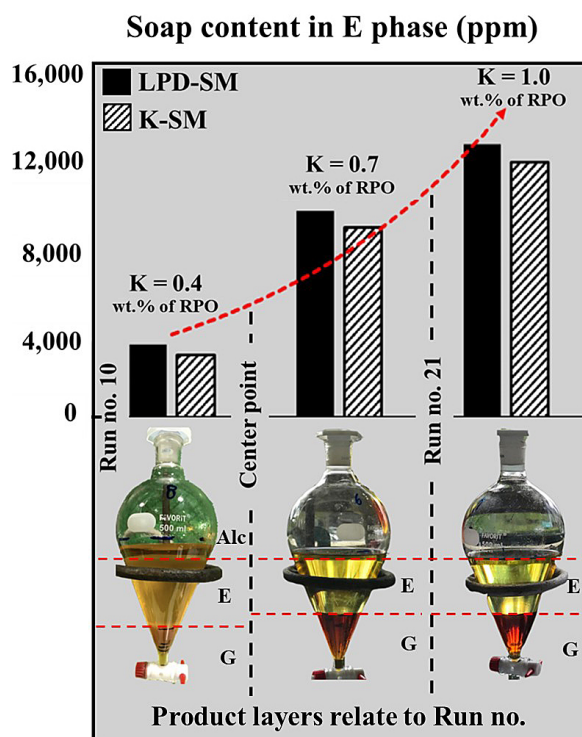


**Figure 5.** The correlation between soap content in ester (E) phase with increasing KOH concentrations and phases separation: Excess of alcohol phase (Alc), Ester phase (E), and Glycerol phase (G)

= 150 cm, and  $T = 6$  min) compared to the center point ( $A = 5:1$  mol MeOH: mol RPO,  $K = 0.7$  wt.% of RPO,  $L = 150$  cm, and  $T = 6$  min), rising from 35.18 up to 85.13 wt.% (85.13 was the average %E from the center point) for LPD-SM, and for K-SM from 29.35 to 84.19 wt.% (84.19 was the average %E from the center point). It is intuitively clear that the early addition of KOH concentration resulted in an increased %E.

However, an increase in KOH concentration, after reaching a certain catalyst concentration ( $K \geq 0.9$  wt.%), %E started to decrease for both mixing elements. The comparison involved increasing the KOH concentration from the center point to run no. 21 ( $A = 5:1$  mol MeOH: mol RPO,  $K = 1.0$  wt.% of RPO,  $L = 150$  cm, and  $T = 6$  min), where a higher KOH concentration led to a decrease in %E from 85.13 to 82.59 for LPD-SM and from 84.19 to 81.38 wt.% for K-SM. This phenomenon was attributed to a more concentrated KOH exceeding 0.9 wt.% of RPO, aligning with the findings in the study involving homogeneous KOH in the transesterification reaction. As the KOH concentration approached 1 wt.% of RPO, a decreasing trend in %E was observed [38].

The excess KOH concentration led to poor mixing solution [38] and resulted in elevated soap formation [13, 40]. The analysis in Figure 5 demonstrates a notable increase in soap content with higher KOH concentrations in E phase. The soap formed a thick barrier shell that hindered the easy diffusion of reactants, consequently reducing the overall reaction rate. Additionally, research has corroborated the adverse effects of high catalyst concentrations, including the presence of unused catalysts due to increased mass transfer resistance and viscosity issues in the mixture [22]. These findings underscore the critical importance of precise control over these parameters in transesterification processes with DPSM for optimal yields and efficiency.

#### *The interaction effect between the molar ratio of MeOH to RPO and residence time*

Figure 4(c) and Figure 4(d) illustrated the 3D response surface plot of %E resulting from the interaction of the molar ratio of MeOH to RPO against residence time for LPD-SM and K-SM, respectively. These graphs were plotted while the other parameters were maintained at their center point ( $K = 0.7$  wt.% of RPO and  $L = 150$  cm). In this context, %E significantly increased from 2 to 7.5 min in LPD-SM and from 2 to 7 min for K-SM with any increase in methanol within the range of 4:1 to 6:1 mol MeOH: mol RPO. As is well-known, transesterification is a fast reaction [30] due to its ability to convert a substantial amount of TG in a short time. After this initial phase, the reaction rate decreases due to the depletion of TG in RPO. This leads to %E remaining constant and exhibiting a decreasing trend beyond that range, as depicted in the contour plot in Figure 4(g) and Figure 4(h) for LPD-SM and K-SM, respectively.

The decrease in %E observed in the contour plot for residence times beyond this range may be attributed to a shift in the reaction equilibrium to the left. For instance, free glycerol may react with methyl esters to form TG [22]. However, when considering the residence time compared to the traditional reactor (CSTR), which requires an optimal residence time of  $\geq 60$  min [8, 22] to achieve %E > 96.5 wt.%, mixing elements type LPD-SM ( $A = 5.5:1$  mol MeOH: mol RPO,  $K = 0.9$  wt.% of RPO,  $L = 200$  cm, and  $T = 8$  min) demonstrated an advantage over CSTR at the same set-point, reducing the residence time by about seven times.

## Optimal conditions for DPSM

This study investigated the comparative maximum and optimal conditions for both LPD-SM and K-SM processes. The maximum conditions, derived from actual experiments, were compared with those predicted by the regression model (optimal conditions). Under the maximum conditions, LPD-SM and K-SM achieved %E values of 96.64% and 96.46 wt.%, respectively. However, it's noteworthy that K-SM fell short of meeting the commercial standard for %E (EN 14214), which requires exceeding 96.5%. Consequently, the optimal conditions predicted by the model were utilized to identify the settings that would yield %E greater than 96.5 wt.%. The outcomes for both sets of conditions are presented in Table 8. To validate the optimal conditions determined by the predicted %E, TLC/FID was employed to assess %E. Consequently, %E values of 96.73 wt.% for LPD-SM and 96.56 wt.% for K-SM were achieved in the actual experiment. The corresponding data from TLC/FID for both mixing elements are presented in Table 9.

Table 10 illustrates the performance of different reactors used for biodiesel production through transesterification using an alkaline catalyst, compared with the optimal conditions of LPD-SM and K-SM from this research. The comparison of %E of LPD-SM and K-SM in this work shows advantages over all single-step

traditional biodiesel production reactors in terms of significantly reducing time and chemical consumption. Additionally, the comparison of other SMs with the LPD-SM in this study reveals higher performance in terms of reducing SM length while achieving the same set point at %E > 96.5 wt.% [28].

## Fuel properties of the optimal conditions

The fuel properties from the optimal conditions of LPD-SM and K-SM were tested, as indicated in Table 11, and complied with the limits set by the EN14214 standards.

## CONCLUSIONS

In conclusion, the results indicate that LPD-SM can be effectively utilized for actual biodiesel production. LPD-SM exhibits an advantage over K-SM, showing a lower consumption of alcohol and catalyst while achieving the same predicted %E. Statistical analysis reveals that the KOH concentration (K) was the most significant factor among the considered independent variables, followed by residence time (T), SM length (L), and the molar ratio of MeOH to RPO (A). The challenges related to dilution solutions and poor mixing solution serve as a cautionary note for biodiesel production with DPSM.

**Table 8.** The conditions of transesterification process with DPSM

Condition	Units	Maximum condition from actual experiment		Optimal condition from predicted model (96.5 wt.% of %E)	
		LPD-SM	K-SM	LPD-SM	K-SM
Molar ratio of MeOH to RPO (A)	mol: mol	5.5:1	5.5:1	5:1	5.5:1
KOH concentration (K)	wt.% of RPO	0.9	0.9	0.76	0.81
SM length (L)	cm	200	200	250	250
Residence time (T)	min	8	8	7.7	7.2

**Table 9.** Analysis for validating %E with TLC/FID of optimal conditions.

Peaks	LPD-SM			K-SM		
	R.T. (min)	Peak Area	Peak Area (%)	R.T. (min)	Peak Area	Peak Area (%)
1) E	0.132	11,191	96.73	0.115	9,198	96.56
2) TG	0.181	222	1.92	0.156	178	1.87
3) DG	0.293	89	0.77	0.259	71	0.75
4) FFAs	0.315	26	0.22	0.285	32	0.34
5) MG	0.405	41	0.35	0.4	46	0.48
Total ( $\sum A_T$ )		11,569	100		9,525	100

**Table 10.** Comparative of reactor performance for the transesterification of biodiesel

Type of reactor	Reaction conditions				%E (wt.%)	Ref
	Alcohol to oil (mol:mol)	Catalyst	Temperature	Residence time (min)		
Single-step traditional biodiesel production						
Batch Reactor	8:1	NaOCH <sub>3</sub> (1wt.%)	60	45	98.2	[41]
Plug Flow Reactor (PFR)	4.3:1	KOH (1.8 wt.%)	30	30	98.0	[10]
Continuous Stirred Tank Reactor (CSTR)	6:1	KOH (1 wt.%)	60	60	97.3	[24]
Continuous Deglycerolisation Reactor (CDR)	5.5:1	KOCH <sub>3</sub> (1.2 wt.%)	60	30	98.0	[42]
Cavitation Reactor	6:1	KOH (1 wt.%)	40	15	99.4	[43]
Static Mixer (SM)						
Kenics Static Mixer (K-SM) (SM length 480 cm)	10:1	KOH (1.26 wt.%)	60	0.9	96.87	[31]
Lightnin Static Mixer (L-SM) (SM length 100 cm with 15 mixing elements)	5.6:1	KOH (1.34 wt.%)	50	0.6	45.04	[32]
Kenics Static Mixer (K-SM) (SM length 60 cm)	6:1	KOH (1 wt.%)	60	30	N/A	[44]
Low-Pressure Drop Static Mixer (LPD-SM) (SM length 250 cm)	5:1	KOH (0.76 wt.%)	60	7.7	96.73	
Kenics Static Mixer (K-SM) (SM length 250 cm)	5.5:1	KOH (0.81 wt.%)	60	7.2	96.56	

**Table 11.** Fuel properties analysis of optimal conditions

Item	Properties	Units	LPD-SM	K-SM	EN14214	Test method
1	Methyl ester content	wt. %	96.71	96.52	96.5 min	EN 14103
2	Density at 15 °C	kg/m <sup>3</sup>	869	864	860-900	ATM D1298
3	Kinematic viscosity at 40 °C	mm <sup>2</sup> /s	4.64	4.26	3.5-5.0	ASTM D445
4	Flash point	°C	164	168	101 min	ASTM D93
5	Carbon residue	wt. %	0.12	0.1	0.3 max	ASTM D4530
6	Sulphated ash content	wt. %	<0.005	0.015	0.02 max	ASTM D874
7	Water content	wt. %	<0.05	<0.05	0.05 max	EN ISO 12937
8	Methanol content	wt. %	<0.01	<0.01	0.2 min	EN 14110
9	Copper strip corrosion	No.	1a	1a	1 max	ASTM D130
10	Oxidation stability (110 °C)	hr	10.46	10.39	8 min	EN 15751

## Acknowledgement

The authors are grateful to the Department of Chemical Engineering, The Specialized R&D Center for Alternative Energy from Palm Oil and Oil Crops (PSU-Biodiesel), PSU graduate school, PSU Research and Development Office (RDO), Prince of Songkla University, for their continuous support throughout my research endeavor. This work was supported by the Prince of Songkla University Research Grant under [grant number ENG6402065S].

## REFERENCES

- Kabeyi, M.J.B., Olanrewaju O. 2022. Sustainable energy transition for renewable and low carbon grid electricity generation and supply. *Frontiers in Energy Research*, 9, 743114.
- Arshad, S., Ahmad M., Munir M., Sultana S., Zafar M., Dawood S., Rozina., Alghamdi A.M., Asif S., Bokhari A., Mubashir M., Chuah L.F., Show P.L. 2023. Assessing the potential of green CdO<sub>2</sub> nanocatalyst for the synthesis of biodiesel using non-edible seed oil of Malabar Ebony. *Fuel*, 333, 126492.

3. Ergen, G. 2024. Comprehensive analysis of the effects of alternative fuels on diesel engine performance combustion and exhaust emissions: Role of biodiesel, diethyl ether, and EGR, 47, 102307.
4. Gómez-Castro, F.I., Gutiérrez-Antonio C., Romero-Izquierdo A.G., May-Vázquez M.M., Hernández S. 2023. Intensified technologies for the production of triglyceride-based biofuels: Current status and future trends. *Renewable and Sustainable Energy Reviews*, 184, 113580.
5. Masera, K., Hossain A.K. 2023. Advancement of biodiesel fuel quality and NOx emission control technique. *Renewable and Sustainable Energy Reviews*, 178, 113235.
6. Rocha-Meneses, L., Hari A., Inayat A., Yousef L.A., Alarab S., Abdallah M., Shanableh A., Ghenai C., Shanmugam S., Kikas T. 2023. Recent advances on biodiesel production from waste cooking oil (WCO): A review of reactors, catalysts, and optimization techniques impacting the production. *Fuel*, 348, 128514.
7. Zaher, F.A., Soliman H.M. 2015. Biodiesel production by direct esterification of fatty acids with propyl and butyl alcohols. *Egyptian Journal of Petroleum*, 24(4), 439-443.
8. Tabatabaei, M., Aghbashlo M., Dehghani M., Panahi H.K.S., Mollahosseini A., Hosseini M., Soufian M.M. 2019. Reactor technologies for biodiesel production and processing: A review. *Progress in Energy and Combustion Science*, 74, 239–303.
9. Abusweireh, R.S., Rajamohan N., Vasseghian Y. 2022. Enhanced production of biodiesel using nanomaterials: A detailed review on the mechanism and influencing factors. *Fuel*, 319, 123862.
10. Lin, C.Y., Wu X.E. 2022. Determination of cetane number from fatty acid compositions and structures of biodiesel. *Processes*, 10(8), 1502.
11. Mehdaoui, I., Majbar Z., Hassani E.M.S., Mahmoud R., Atemni I., Abbou M.B., Taleb M., Rais Z. 2023. Energy valorization of olive mill waste cake-extraction of vegetable oil and transesterification. *Journal of Ecological Engineering*, 24(5), 306-315.
12. Jalaluddin, J., Ginting Z., Maliki S., Setiawan A., Zulfa Z. 2022. Biodiesel production from crude palm oil using kapok skin KOH (*Ceiba Pentandra*) catalyst as solid green catalyst. *Journal of Ecological Engineering*, 23(5), 286-292.
13. Chanakaewsomboon, I., Moollakorn A. 2021. Soap formation in biodiesel production: effect of water content on saponification reaction. *International Journal of Chemical and Environmental Sciences*, 2(2), 28–36.
14. Takase, M., Bryant I.M., Essandoh P.K., Amankwa A.E.K. 2023. A comparative study on performance of KOH and 32%KOH/ZrO<sub>2</sub>-7 catalysts for biodiesel via transesterification of waste Adansonia digitata oil. *Green Technologies and Sustainability*, 1(3), 100004.
15. Reynoso, A.J., Ayastuy J.L., Iriarte-Velasco U., Gutiérrez-Ortiz M.A. 2023. Bio-hydrogen and valuable chemicals from industrial waste glycerol via catalytic aqueous-phase transformation. *Fuel Processing Technology*, 242, 107634.
16. de Oliveira, V.F., Parente E.J.S., Manrique-Rueda E.D., Cavalcante C.L., Luna F.M.T. 2020. Fatty acid alkyl esters obtained from babassu oil using C<sub>1</sub>–C<sub>8</sub> alcohols and process integration into a typical biodiesel plant. *Chemical Engineering Research and Design*, 160, 224–232.
17. Nogales-Delgado, S., Encinar J.M., González Cortés Á. 2021. High oleic safflower oil as a feedstock for stable biodiesel and biolubricant production. *Industrial Crops and Products*, 170, 113701.
18. Šánek, L., Pecha J., Husár J., Kolomazník K. 2019. Mathematical modeling of transesterification process kinetics of triglycerides catalyzed by TMAH. *MATEC Web of Conferences*, 292, 01027.
19. Zahan, K.A., Kano M. 2019. Technological progress in biodiesel production: An overview on different types of reactors. *Energy Procedia*, 156, 452–457.
20. Pongraktham, K., Somnuk K. 2020. Continuous methyl ester production process from refined palm oil using 3D-printed static mixers. *Materials Science Forum*, 998, 134–139.
21. Nouredini, H., Harkey D., Medikonduru A. 1998. A continuous process for the conversion of vegetable oils into methyl esters of fatty acids. *Journal of the American Oil Chemists' Society*, 75, 1775-1783.
22. Darnoko, D., Cheryan M., 2000. Continuous production of palm methyl esters. *Journal of the American Oil Chemists' Society*, 77, 1269-1272.
23. Qiu, Z., Zhao L., Weatherley L. 2010. Process intensification technologies in continuous biodiesel production. *Chemical Engineering and Processing - Process Intensification*, 49(4), 323-330.
24. Sungwornpatansakul, P., Hiroi J., Nigahara Y., Jayasinghe T.K., Yoshikawa K. 2013. Enhancement of biodiesel production reaction employing the static mixing. *Fuel Processing Technology*, 116, 1–8.
25. Kolmetz, K., Jaya A. 2014. Static mixer selection, sizing and troubleshooting. *KLM technology group, Johor Bahru, Malaysia*.
26. Jiang, X., Xiao Z., Jiang J., Yang X., Wang R. 2021. Effect of element thickness on the pressure drop in the Kenics Static Mixer. *Chemical Engineering Journal*, 424, 130399.
27. Somnuk, K., Wijitsopa K., Prateepchaikul G. 2016. Optimization of the comparative continuous process of ethyl and methyl ester productions using a static mixer reactor: a response surface methodology approach. *Biofuels*, 9, 331–339.

28. Pongraktham, K., Somnuk K. 2020. Effect of length-to-diameter ratio of mixing elements for methyl ester production process. Academic Journal Uttaradit Rajabhat University [Online serial], Retrieved December 5, 2023 <https://ph01.tcithaijo.org/index.php/uruj/article/download/239984/163976/831583>
29. Stec, M., Synowiec P.M. 2015. Analysis of the pressure drop calculation method impact on the accuracy of the experimental results in the Koflo static mixer. Chemical Engineering and Equipment, 54(4), 201-203.
30. Trejo-Zárraga, F., Hernández-Loyo F.D.J, Chavarría-Hernández J.C., Sotelo-Boyás R. 2018. Kinetics of transesterification processes for biodiesel production. In K. Biernat, ed. Biofuels - State of Development. InTech, 149-179.
31. Berkman, P.D., Calabrese R.V. 1988. Dispersion of viscous liquids by turbulent flow in a static mixer. AIChE Journal, 34, 602–609.
32. Meng, H., Meng T., Yu Y., Wang Z., Wu J. 2022. Experimental and numerical investigation of turbulent flow and heat transfer characteristics in the Komax static mixer. International Journal of Heat and Mass Transfer, 194, 123006.
33. Juera-ong, P., 2023. Continuous biodiesel production from palm oil mill effluent using hydrodynamic cavitation reactor. M. Eng. Thesis, Prince of Songkla University, Hat Yai, Songkhla, Thailand.
34. Hazrat, M.A., Rasul M.G., Khan M.M.K., Ashwath N., Silitonga A.S., Fattah I.M.R., Mahlia T.M.I. 2022. Kinetic modelling of esterification and transesterification processes for biodiesel production utilising waste-based resource. Catalysts, 12, 12111472.
35. Kanjaikaew, U., Tongurai C., Chongkhong S., Prasertsit K. 2018. Two-step esterification of palm fatty acid distillate in ethyl ester production: Optimization and sensitivity analysis. Renewable Energy, 119, 336–344.
36. Khiowthong, W., Thaiyasuit P. 2023. Continuous ethyl ester production in a high-performance rotor reactor at 3:1 molar ratio using response surface methodology. International Energy Journal, 23, 173–186.
37. Abdallah, R.I., Samy B.E.H., Sherif A., Mohamed A.B., Salem S.A.A., Nour S.E.G., Mohamed S.A., Nagwa M.S. 2017. Optimization of a batch CaO-catalyzed transesterification of used domestic waste oil with methanol and elucidation of a mathematical correlation between biodiesel yield and percent conversion. Energy Sources, Part A: Recovery, Utilization, and Environmental Effects, 7230.
38. Agarwal, M., Chauhan G., Chaurasia S.P., Singh K. 2012. Study of catalytic behavior of KOH as homogeneous and heterogeneous catalyst for biodiesel production. Journal of the Taiwan Institute of Chemical Engineers, 43, 89–94.
39. Mohammadi, N., Ostovar N., Niromand R., Absalan F. 2023. Advancing biodiesel production from *Pyrus glabra* seed oil: Kinetic study and RSM optimization via microwave-assisted transesterification with biocompatible hydroxyapatite catalyst. Sustainable Chemistry and Pharmacy, 36, 101272.
40. Chanakaewsomboon, I., Phoungthong K., Palamanit A., Seechamnaturakit V., Cheng C.K. 2021. Biodiesel produced using potassium methoxide homogeneous alkaline catalyst: effects of various factors on soap formation. Biomass Conversion and Biorefinery, 13(10), 1–11.
41. Sharma, Y.C., Singh B., Korstad J. 2010. High yield and conversion of biodiesel from a nonedible feedstock (*Pongamia pinnata*). Journal of Agricultural and Food Chemistry, 58, 242-247.
42. Nikhom, R., Tongurai C. 2014. Production development of ethyl ester biodiesel from palm oil using a continuous deglycerolisation process. Fuel, 117b, 926-931.
43. Thipdech, A., Prasertsit K., Photaworn S. 2024. Process intensification of biodiesel production using pilot-scale continuous multiple baffle reactor with feed distribution. Chemical Engineering and Processing-Process Intensification, 195, 109614.
44. Thompson, J.C., He B.B. 2007. Biodiesel production using static mixers. Transactions of the American Society of Agricultural and Biological Engineers, 50, 161–165.